

New High-Temperature Pb-Catalyzed Synthesis of Inorganic Nanotubes

Olga Brontvein,[†] Daniel G. Stroppa,[‡] Ronit Popovitz-Biro,[§] Ana Albu-Yaron,[†] Moshe Levy,[†] Daniel Feuerman,^{||} Lothar Houben,[‡] Reshef Tenne,^{*,†} and Jeffrey M. Gordon^{||,⊥}

[†]Department of Materials and Interfaces, Weizmann Institute of Science, P.O. Box 26, Rehovot 76100, Israel

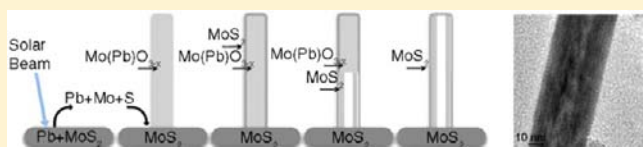
[‡]Institute of Solid State Research and Ernst Ruska Centre for Microscopy and Spectroscopy with Electrons, Forschungszentrum Jülich GmbH, Germany

[§]Electron Microscopy Unit, Weizmann Institute of Science, P.O. Box 26, Rehovot 76100, Israel

^{||}Department of Solar Energy and Environmental Physics, Jacob Blaustein Institutes for Desert Research, Ben-Gurion University of the Negev, Sede Boqer Campus 84990, Israel

[⊥]The Pearlstone Center for Aeronautical Engineering Studies, Department of Mechanical Engineering, Ben-Gurion University of the Negev, Beersheva 84105, Israel

ABSTRACT: A new procedure for the synthesis of MoS₂ nanotubes is reported, and additionally demonstrated for MoSe₂, WS₂, and WSe₂. Highly concentrated sunlight creates continuous high temperatures, strong temperature gradients, and extended hot annealing regions, which, together with a metallic (Pb) catalyst, are conducive to the formation of different inorganic nanotubes. Structural characterization (including atomic resolution images) reveals a three-step reaction mechanism. In the first step, MoS₂ platelets react with water–air residues, decompose by intense solar irradiation, and are converted to molybdenum oxide. Subsequently, the hot annealing environment leads to the growth of Pb-stabilized MoO_{3-x} nanowiskers. Shortly afterward, the surface of the MoO_{3-x} starts to react with the sulfur vapor supplied by the decomposition of nearby MoS₂ platelets and becomes enveloped by MoS₂ layers. Finally, the molybdenum oxide core is gradually transformed into MoS₂ nanotubes. These findings augur well for similar syntheses of as yet unattained nanotubes from other metal chalcogenides.



1. INTRODUCTION

1.1. Transition Metal Chalcogenide Fullerene-like Nanoparticles and Nanotubes. The study of inorganic nanometer-scale materials with hollow closed-cage structures is a rapidly growing field. The first inorganic fullerene-like nanoparticles (IF) and nanotubes (INT) of WS₂¹ and MoS₂² were obtained by heating thin metal films (W or Mo) in the presence of gaseous H₂S. The MX₂ compounds (M = W, Mo; X = S, Se) crystallize in a layered structure (space group P6/m3) that belongs to the transition metal chalcogenide (TMC) family. A variety of layered TMCs such as TiS₂, NbS₂,^{3,4} TaS₂,^{3,5} and other inorganic layered materials^{6–9} have demonstrated the ability to form IF/INT structures, and a number of synthetic routes have been developed, for example, chemical vapor transport using bromine for INT-MoS₂,^{10,11} a bismuth-catalyzed vapor–liquid–solid method for SnS₂ nanotubes¹² and superstructure SnS–SnS₂ nanotubes.¹³

1.2. Prior Syntheses of MoS₂ and WS₂ Nanotubes. The most promising method for high yields of almost defect-free IF-MoS₂, IF-WS₂ IF and INT-WS₂ is sulfidization of the respective metal oxides under reducing conditions. For IF-WS₂, WO₃ spherical nanoparticles were used as solid precursors^{14,15} in a process where the reaction temperature was lower than the sublimation temperature of WO₃, so that the kinetically controlled reaction proceeded according to a solid–gas

mechanism. INT-WS₂ were also prepared by a two-step sulfidization of WO_{3-x} nanoparticles at 800–900 °C:¹⁶ (1) the rapid growth of long nonvolatile W₁₈O₄₉ nanowiskers followed by (2) sulfidization under reducing conditions in the same reactor. This solid oxide, with monoclinic space group (P12/m1), consists of an ordered 2-D lattice of edge-sharing WO₆ octahedra forming a network of pentagonal columns (PC) interspersed with hexagonal channels.^{17,18} This phase exhibits preferential growth as elongated nanowiskers that can be converted into INT-WS₂ by fine-tuning the sulfidization reaction. These studies paved the way for the synthesis of WS₂ nanotubes in macroscopic amounts of a few hundred grams per batch.

Recently, small quantities of IF-MoS₂ of about 1 g/day with limited size control were synthesized by vaporizing and subsequently sulfidizing MoO₃ powder.^{19,20} Other groups have synthesized INT-MoS₂ in appreciable amounts and studied their catalytic reactivity.²¹ On the basis of lessons learned from INT-WS₂ syntheses, the main obstacle for obtaining INT-MoS₂ from the respective oxide is the lack of an anisotropic MoO_{3-x} phase that could potentially promote the growth of nonvolatile MoO_{3-x} nanowiskers in a high-

Received: July 18, 2012

Published: September 11, 2012

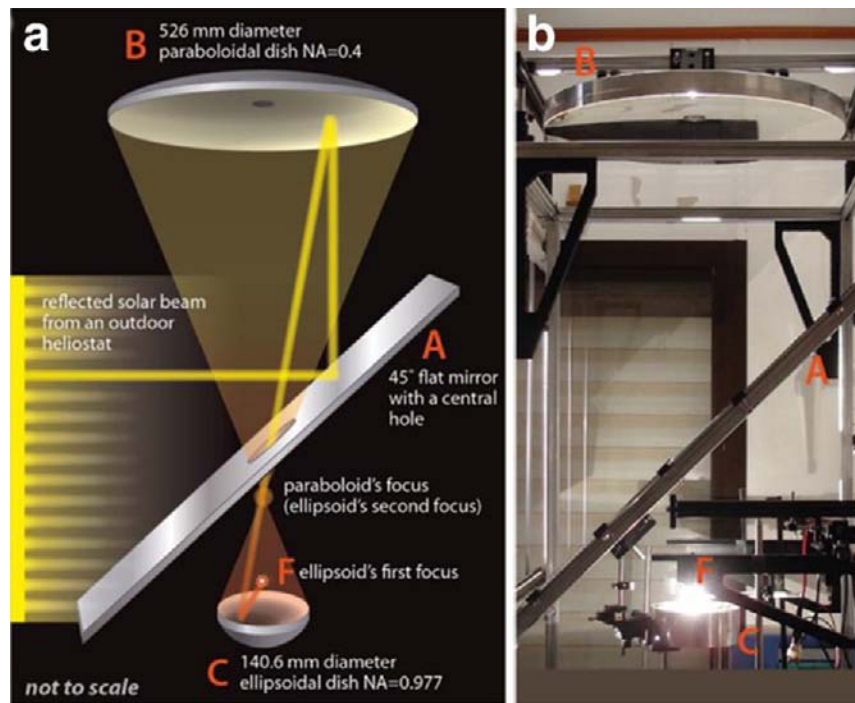


Figure 1. Schematic (a) and photo (b) of our solar furnace. Solar radiation is reflected into the lab from an outdoor heliostat, reflected upward by a flat mirror tilted at 45° (A) to a parabolic dish (B), concentrated through a hole in the flat tilted mirror (A), and further concentrated by an ellipsoidal dish (C) to the focus (F) where the ampule is inserted. Reproduced with permission from ref 47. Copyright 2011 Wiley-VCH.

temperature reaction. MoO_2 nanowiskers and nanotubes were obtained by flame heating of a molybdenum tip at 2500 °C in an acetylene–oxygen rich atmosphere^{22,23} where the high temperature, strong temperature gradient and chemical environment promoted the growth of 1-D nanostructures.

1.3. The Molybdenum Oxide Pathway to MoS_2 Nanoparticles. At high temperatures, MoO_3 exhibits a series of phase changes, involving nonstoichiometric compounds, while being reduced to MoO_2 . First, the partial release of oxygen from MoO_3 allows the formation of crystal shear (CS) planes. The lowest suboxide phase with CS is $\text{Mo}_{18}\text{O}_{52}$.²⁴ Further reduction in the oxygen content of the suboxides leads to the appearance of a phase with pentagonal columns (PC) as the dominant structural motif in both Mo_5O_{14} and the more stable $\text{Mo}_{17}\text{O}_{47}$. In the more reduced suboxide phase Mo_4O_{11} , Mo_6 octahedra are corner-linked to Mo_4 tetrahedra.²³

In this respect, one may consider the tetragonal Mo_5O_{14} ($P4/mbm$) and the orthorhombic $\text{Mo}_{17}\text{O}_{47}$ phase ($Pba2$)²⁵ as the respective analogs of the tetragonal W_5O_{14} ($P\bar{4}21m$) and the more stable monoclinic $\text{W}_{18}\text{O}_{49}$ phase ($P12/m1$), which grow as nanowiskers in a reducing atmosphere. In analogy to the tungsten phases, the Mo_5O_{14} and $\text{Mo}_{17}\text{O}_{47}$ phases possess interspersed CS and PC. The more stable $\text{W}_{18}\text{O}_{49}$ was found to serve as the intermediate asymmetric phase for the synthesis of INT- WS_2 .²⁶ However, the asymmetric $\text{Mo}_{17}\text{O}_{47}$ phase is unstable at high temperatures, decomposing at 560 °C.²⁷

1.4. Metal Catalysis. Previously, Yamazoe et al. reported that vanadium substitution stabilizes the $\text{Mo}_{17}\text{O}_{47}$ phase.²⁸ Similarly, the Mo_5O_{11} phase could be stabilized by adding minute amounts of titanium, niobium and tantalum.^{25,29} Hence, it was hypothesized that different metals which stabilize asymmetric MoO_{3-x} phases could lead to the growth of nanowiskers and, subsequently, INT- MoS_2 .

Metal catalysts are widely used for promoting the growth of 1-D nanoparticles. The most common method is vapor–liquid–solid growth, yielding various nanowires,^{30,31} carbon nanotubes³² and INT^{12,33} with good control of their composition and dimensions. The synthesis of carbon nanotubes has also been realized using homogeneous metal catalysts.^{34,35}

The most common methods for sulfidization of metal oxide powder involve using H_2S gas, which is flammable and toxic, in a reducing atmosphere. Furthermore, the generation of metal selenide and metal telluride nanoparticles requires even more toxic and unstable precursors. These observations motivate the search for other sources of sulfide (selenide and telluride), as well as alternative synthetic techniques.^{36,37}

1.5. Solar Ablation. Solar ablation as a technique for IF/INT synthesis offers the advantage of permitting a large reaction volume in combination with a high vapor pressure of the reactants at reactor temperatures up to ~3000 K with an ultrahot annealing environment. Moreover, sharp gradients in heat flux and temperature are created, estimated as high as 10^4 K/cm.³⁸ This method has been employed successfully for the synthesis of carbon fullerenes,^{39–42} carbon nanotubes,^{43,44} and an assortment of inorganic nanoparticles.^{36,38,45–47}

Here, a solar furnace (Figure 1) is exploited to drive highly anisotropic and kinetically controlled reactions for synthesizing molybdenum oxide nanowiskers and MoS_2 nanotubes. To wit, a new Pb-catalyzed method to synthesize nanotubes from different metal dichalcogenide nanoparticles using high-temperature solar ablation is reported, along with the elucidation of its multistep reaction mechanism. The experimental realization of this procedure and deciphering the reaction pathway opens up new vistas, creating new possibilities for the synthesis of yet-unrealized nanotubes from different metal chalcogenide compounds.

Reactor temperatures can be estimated from known threshold temperatures for syntheses achieved in the same solar ablation facility.^{38,47} One example is the production of carbon nanotubes from pure graphite without catalysis, invariably requiring the sublimation of graphite and hence reactor temperatures reaching ~ 2700 K. Additional evidence includes both (1) synthesizing MoS₂ nano-octahedra in a procedure which requires the vaporization of Mo at temperatures of at least ~ 2700 K, as well as (2) the generation of SiO₂ nanowires and nanospheres via the melting and possible vaporization of pure quartz. Determination of reactor temperature is hindered by the blinding effect of concentrated solar radiation reflected off the quartz reactor ampules, as well as the paucity of suitable thermocouple materials. (Developing a noninvasive method to ascertain reactor temperature is a work in progress.)

2. EXPERIMENTAL SECTION

2.1. Sample Preparation and the Solar Furnace. Quartz ampules (12 mm o.d.) were filled with different precursors and sealed under a vacuum of 3×10^{-5} Torr. All precursors included a TMC (MoS₂ (99%, Alfa Aesar), WS₂ (99.8%, Alfa Aesar), MoSe₂ (99.9%, Strem) or WSe₂ (99.8%, Alfa Aesar)) and a metal catalyst in a 1:1 molar ratio. Some precursor mixtures included pure Pb (99.5%, Strem), while others contained a powder consisting of crystallites with a core of pure Pb coated with PbO film in the ratio 40/60 at %. Experiments in which pure PbO powder (99.9%, Acros) was used did not yield the novel nanoparticles detailed below.

The ampules were irradiated during exposure times of 30–1200 s by highly concentrated solar beam radiation. A flux concentration of up to $\sim 15\,000$, that is, 15 W/mm^2 , on a focal spot a few mm^2 in area was attained in a solar furnace delineated previously³⁸ (a schematic and photograph are shown in Figure 1).

2.2. Electron Microscopy. The solar ablated samples were examined by electron microscopy techniques, primarily with a Philips CM120 transmission electron microscope (TEM) operating at 120 kV, equipped with an energy-dispersive X-ray spectroscopy (EDS) detector for chemical analysis (EDAX Phoenix Microanalyzer), and secondarily with an LEO model Supra 55VP scanning electron microscope (SEM) equipped with an EDS detector (Oxford model INCA). High-resolution imaging was achieved with an FEI Tecnai F30-UT with a field-emission gun operating at 300 kV. Line-scan EDS analysis was performed with an FEI Tecnai F20 scanning transmission electron microscope (STEM), operating at 200 kV, equipped with a high-angle annular dark field (HAADF) detector and EDS detector (EDAX-Phoenix Microanalyzer). For atomic resolution analysis, a probe aberration-corrected FEI Titan 80-300 STEM operating at 300 kV equipped with a high-angle annular dark field (HAADF) detector was used.

3. RESULTS AND DISCUSSION

3.1. MoS₂: Scanning and Transmission Electron Microscopy and Electron Diffraction Analysis. After irradiation of the MoS₂ and Pb mixture for 600 s, MoS₂ nanotubes were readily apparent (Figure 2), mainly with one closed and one open end. The TEM (Figure 2a) and SEM (Figure 2b) images show nanotubes growing from MoS₂ platelets. The nanotubes were partially filled with a MoO_{3-x} core of nonuniform thickness. Most of the oxide remained near the nanotube's closed end, while the amount of oxide near the nanotube root was much smaller. This observation suggests that the conversion of the oxide nanowhirsker to INT-MoS₂ by reaction with sulfur vapor emanates from the root. Nanotube dimensions ranged from 100 nm to 1 μm in length, and from 15 to 80 nm in width. The number of layers varied from two (encapsulating a MoO_{3-x} core) to more than 30 (for the fully

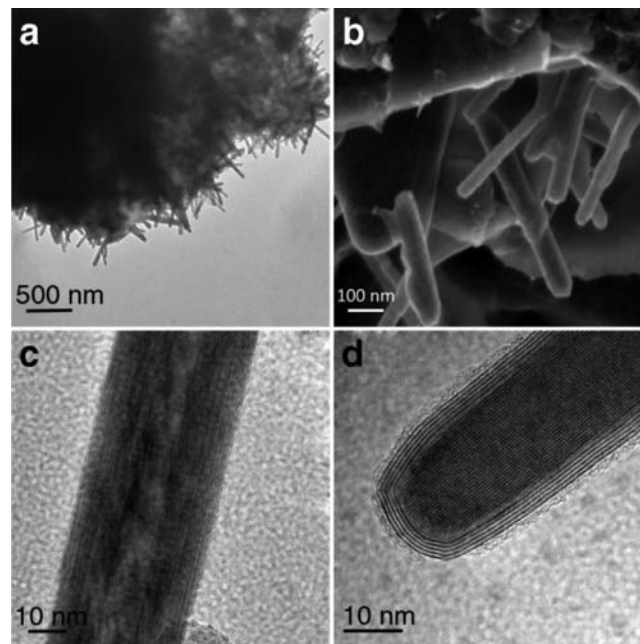


Figure 2. Electron microscopy of representative MoS₂ nanotubes after exposure of MoS₂ and Pb mixture for 600 s. (a) Lower magnification TEM image. (b) SEM image. (c) High-magnification TEM image of a single hollow MoS₂ nanotube. (d) High-magnification TEM image of a filled MoS₂ nanotube.

converted hollow core zones). According to the EDS analysis in the TEM, these nanotubes consist of Mo, S, traces of Pb ($\sim 1\text{--}5$ at %) and, in some cases, O (Table 1). The Pb content is progressively reduced, eventually reaching below 1 at % with the gradual conversion of the oxide core into closed MoS₂ layers. Careful SEM/TEM analyses revealed that nanotubes could not be obtained from any of the precursors in the absence of Pb, or by replacing the atomic Pb with PbS or PbO.

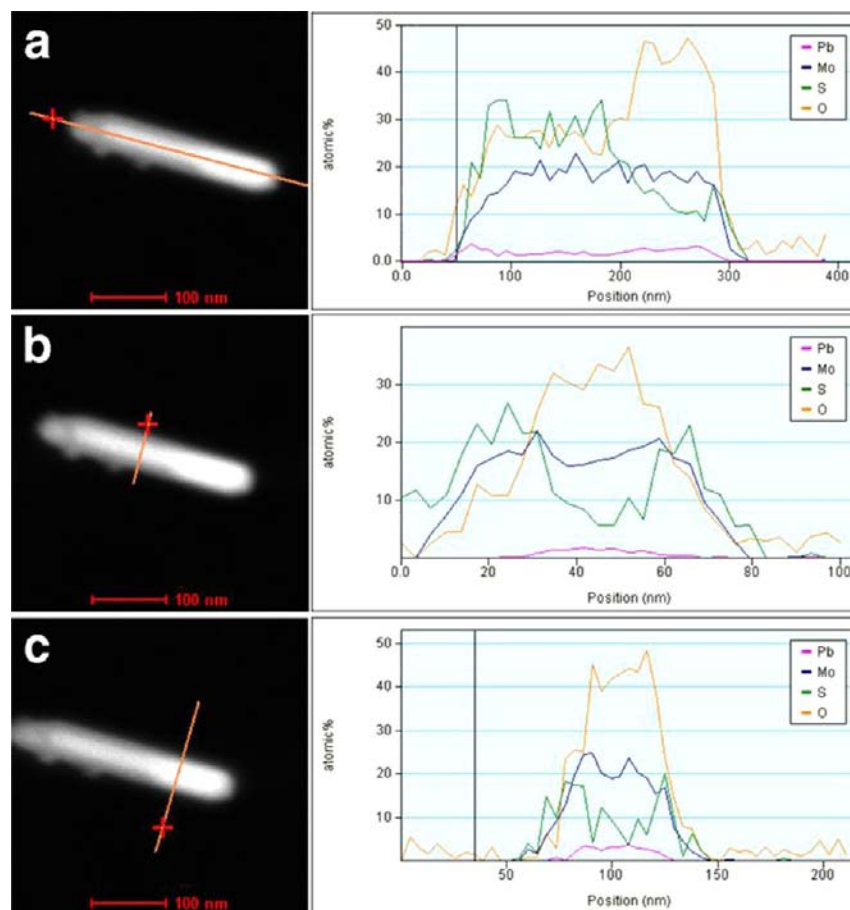
Nanotube yields on the surface of the MoS₂ crystallites were high (see Figure 2), but only in certain zones. Overall yields (averaged over the reactor) did not exceed a few percent, which is not surprising given the large nonuniformities inherent to these experiments. Nonetheless, the experimental results (including the representative nanostructures shown in the Figures and the nanotube yields) were reproducible. The main obstacles for achieving higher yields were: (1) The reactions were basically restricted to the irradiated region of the powder's surface. (2) The irradiated powder was stationary (rather than fluidized), precluding mixing during the reaction. (3) To avert shattering of the ampule, the irradiation period was limited to 10–30 min. The combined effect of these exigencies leaves considerable room for future improvements in nanotube yield.

Scaling up nanotube production will require a far larger focal region, combined with full automation of mixing and fluidizing the powder. Because of the current relatively low yield of the nanotubes, characterization of the products is limited to electron microscopy methods. Methods such as X-ray diffraction and X-ray photoelectron spectroscopy will be used once the overall yield of the process is improved along the guidelines noted above.

A line-scan EDS of a single MoS₂ nanotube illuminates the distribution of Pb (Figure 3). The nanotube core is filled with variable amounts of MoO_{3-x} along its growth axis. The closed end consists mostly of the MoO_{3-x} core encapsulated by a few layers of MoS₂, whereas the open end is composed mostly of

Table 1. TEM/EDS Analysis of Representative Nanoparticles

Sample	INT-MoS ₂ (filled)	INT-MoS ₂ (hollow)	MoO _{3-x}
Image			
O [at%]	25	17.2	61.4
S [at%]	37.5	50.5	4.8
Pb [at%]	3.3	1	6.2
Mo [at%]	34.2	31.3	27.6

**Figure 3.** Line-scan EDS of a single MoS₂ nanotube with partially filled oxide core. (a) Along the nanotube axis. Transverse strips with (b) a small amount of MoO_{3-x} and several MoS₂ layers, and (c) a MoO_{3-x} interior encased by a few MoS₂ shells.

MoS₂ layers filled with a smaller amount of MoO_{3-x}. The Mo, S, and O line profiles are consistent with the described structure. The small Pb content of the nanostructure has a line profile indicating a homogeneous distribution throughout the MoO_{3-x} core, falling below the detection limit in the MoS₂ shell.

Aberration-corrected TEM revealed a small number of Pb atoms substituting for the Mo atoms in the MoS₂ lattice. Additionally, Pb atoms were found advancing in the oxide core at the growth front of the MoS₂ layers. This observation indicates that the Pb atoms, which are essential for the high-

temperature stability of the oxide nanowhiskers, are ejected or “salted out” by the growing MoS₂ layer. Given the large difference between the solubility of Pb in the oxide and sulfide phases, one would expect to find some Pb-rich grains within or near the nanotube. The absence of such grains indicates that the Pb atoms are swept away as a vapor from the growing nanotube or form an unidentified chemical compound. However, it is evident from the high resolution aberration-corrected STEM analysis that some of the remaining Pb atoms replace Mo atoms. Figure 4 shows a representative HAADF

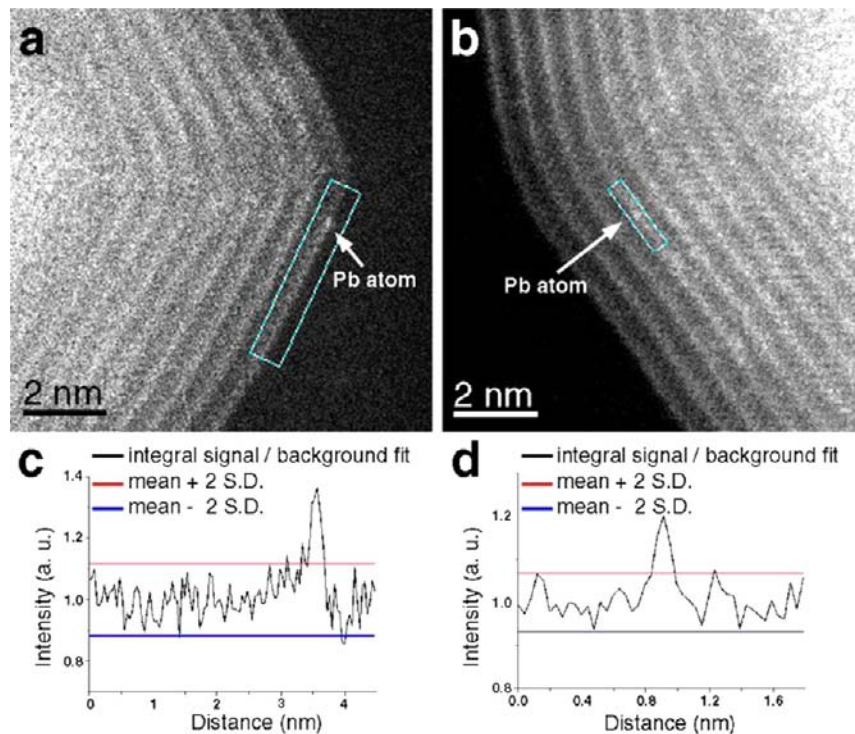


Figure 4. (a and b) High-resolution aberration-corrected HAADF image of a single MoS_2 nanotube. (c and d) Normalized line profile data taken from the marked layers in the HAADF images. The profile data are normalized to the signal intensity of MoS_2 layers lacking extraordinary bright dots. Signal enhancements (SE) significantly beyond background noise (horizontal lines) can be identified as individual Pb atoms.

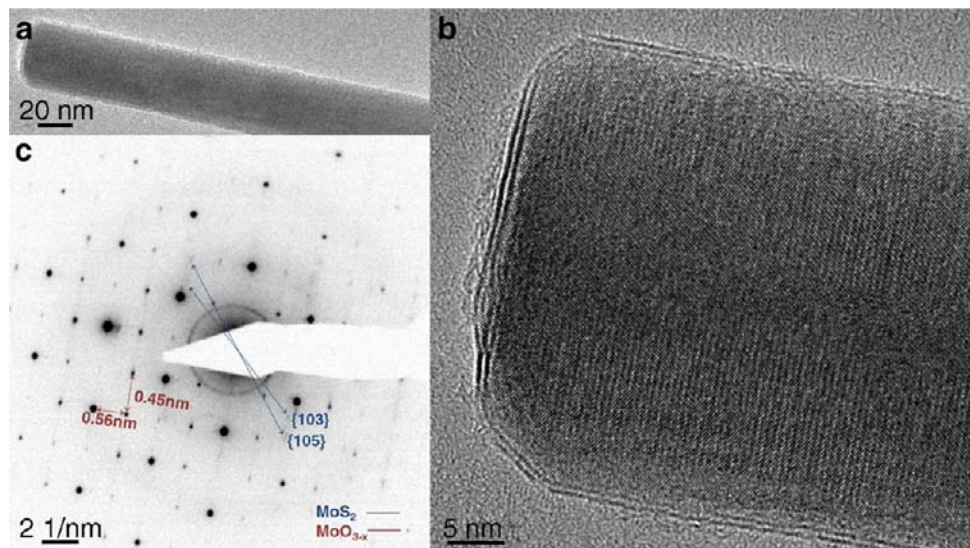


Figure 5. Characterization of a single MoS_2 nanotube with a crystalline oxide core. (a) Low magnification TEM image. (b) High-resolution TEM image. (c) ED pattern.

image, where residual Pb atoms appear as bright spots in the MoS_2 lattice. Normalized line profile data were used to unequivocally identify the Pb signal against the background signal of MoS_2 , thus clearly distinguishing between the Mo atoms and individual Pb atoms (Figure 4c,d). The density of individual Pb atoms in the MoS_2 lattice is low and in agreement with a concentration of less than 1% at.

The electron diffraction (ED) pattern of a single MoS_2 nanotube (Figure 5) has two sets of points that belong to two different structures (lattices). The two pairs of bright spots marked with blue arrows belong to the MoS_2 phase. The

points appropriate to a single-crystal structure correspond to MoO_{3-x} in a phase that cannot be defined based on its d -spacing due to the large number of molybdenum suboxide phases commensurate with these distances. In addition, the powder diffraction files of pure $\text{Mo}_{17}\text{O}_{47}$ and vanadium-stabilized $\text{Mo}_{17}\text{O}_{47}$ reveal modified d -spacings due to the vanadium-induced strain. The conclusion is that Pb atoms can also change the d -spacings in some molybdenum suboxide phases. The existence of a MoO_{3-x} phase in the core of the nanotube suggests that the water molecules which react with the molybdenum sulfide to form molybdenum oxide produce a

hydrogen atmosphere conductive to the high-temperature reduction of the trioxide to the suboxide phase in the nanowhisker core.

3.2. Deciphering the MoS_2 Nanotube Formation Mechanism.

Mechanism. Limiting the solar exposure time to 30 s revealed the generation of MoO_{3-x} nanowhiskers (Figure 6a). After 60 s,

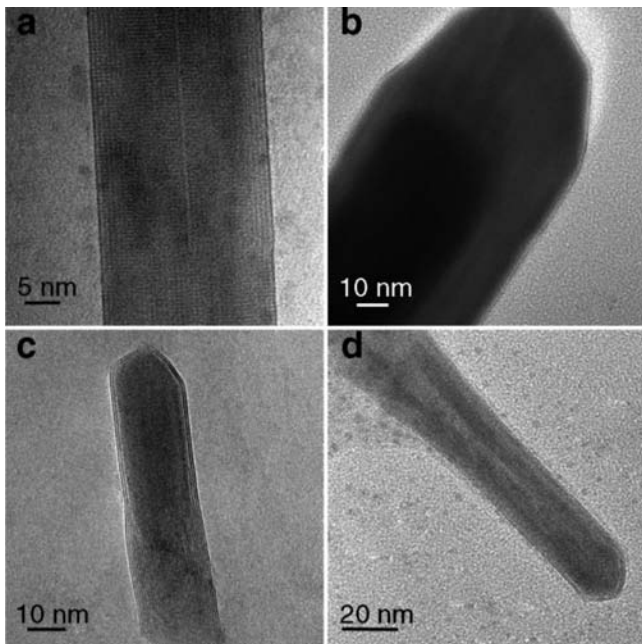


Figure 6. TEM images highlighting the temporal evolution of MoO_{3-x} and MoS_2 nanoparticles for varying periods of solar irradiation. (a) MoO_{3-x} nanowhisker after 30 s. (b) MoO_{3-x} nanowhisker covered by a single layer of MoS_2 after 60 s. (c) MoS_2 nanotube partially filled with MoO_{3-x} after 600 s. (d) Hollow core MoS_2 nanotube after 1200 s.

one to two layers of MoS_2 surround the MoO_{3-x} nanowhisker (Figure 6b). Progressively longer irradiation periods reveal a continuous transformation of the MoO_{3-x} nanowhiskers to INT- MoS_2 (Figure 6c,d). The EDS analysis reveals 1–5 at % of Pb inside the nanoparticles, throughout the oxide (nanowhiskers), a presence that persists throughout the sulfide (nanotube) conversion. However, the concentration of Pb is noticeably smaller in the sulfide layers than in the molybdenum oxide core.

The growth of MoS_2 nanotubes can be described by a three-step process, shown schematically in Figure 7. In the first step, intense radiative heating rapidly evaporates MoS_2 platelets and Pb particles. A reaction of the hot Mo (and S) vapor with the surrounding gas phase during the next few seconds, especially with the remaining oxygen and water vapor that outgas from the quartz ampule, promotes the growth of fully crystalline MoO_{3-x} nanowhiskers. Since they serve as templates for nanotube growth, that is, for oxide-to-sulfide conversion, the nanowhisker size dictates the nanotube size. The Pb atoms appear to stabilize the MoO_{3-x} nanowhisker phases that are eventually transformed to INT- MoS_2 . It is not unlikely though that the Pb atoms also serve as catalysts for the chemical reaction converting the MoS_2 powder into MoO_{3-x} nanowhiskers. In the second step, during the ensuing minutes, a concerted surface reaction leads to the engulfment of MoO_{3-x} nanowhiskers by a continuous shell consisting of 2–3 MoS_2 layers. In the third step, the inner MoO_{3-x} phase continuously transforms into MoS_2 starting from the base of MoS_2 platelets and progressing to their closed end. The slow conversion of the oxide nanowhisker core into MoS_2 nanotubes is critically dependent on the proximity to the MoS_2 platelets, which, under intense heating, gradually decompose, supplying the sulfur-rich atmosphere.

Numerous attempts to synthesize MoS_2 nanotubes in a conventional oven (up to 1000 °C) or induction furnace (up to 1600 °C), with the same precursor materials, did not yield nanotubes; neither did solar ablation of MoO_3 powder mixed with Pb and S. It appears, therefore, that the high temperatures (up to ~3000 K), pronounced temperature gradients, and hot extended annealing regions created in the solar furnace are critical for MoS_2 nanotube growth from precursor MoS_2 .

The success of solar ablation in the Pb-mediated generation of MoS_2 nanotubes and the elucidation of their growth mechanism prompted attempting the same procedure for MoSe_2 , WS_2 and WSe_2 (vide infra). Attempts to synthesize the respective metal-telluride nanotubes have been unsuccessful so far. However, a new variation of the present approach whereby the oxide whiskers are produced first, and subsequently annealed in a chalcogen atmosphere, will be presented in a forthcoming publication, and could also lead to the synthesis of metal (Mo, W) telluride and other chalcogenide nanotubes. As for other kinds of nanotubes, more research is needed to explore these opportunities.

3.3. MoSe_2 . Solar ablation succeeded in generating INT- MoSe_2 when MoSe_2 powder and Pb were irradiated in an

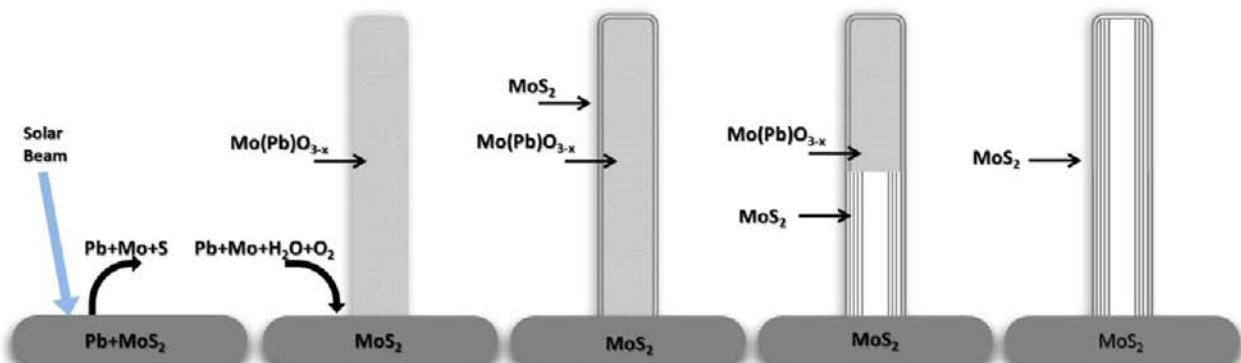


Figure 7. Schematic of the formation mechanism of MoS_2 nanotubes.

evacuated ampule for 600 s (Figure 8). The MoSe₂ nanotubes had dimensions comparable to those of MoS₂, containing a small amount of Pb, and being partially filled with MoO_{3-x}.

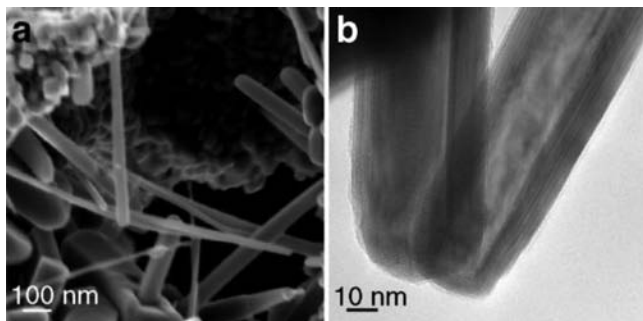


Figure 8. MoSe₂ nanotubes after irradiation of the precursors for 600 s. (a) SEM image. (b) TEM images.

3.4. WS₂. Solar ablation for 600 s also yielded WS₂ nanotubes partially filled with WO_{3-x} (Figure 9) and traces of Pb. The nanotubes were ~50 nm wide, with lengths varying from 100 nm to more than 10 μ m. The number of WS₂ layers varied from 2 to more than 10.

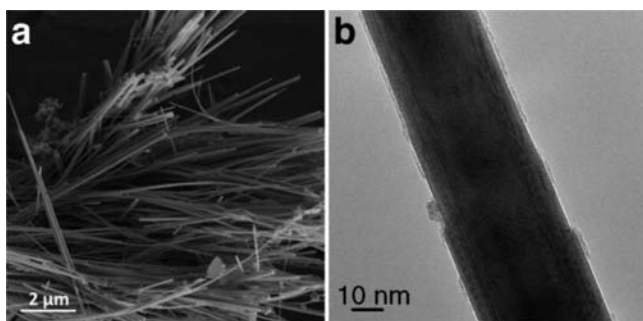


Figure 9. WS₂ nanotubes after the irradiation of the precursors for 600 s. (a) SEM image. (b) TEM image.

3.5. WSe₂. Solar ablation of WSe₂ and Pb for 600 s yielded both hollow WSe₂ nanotubes as well as nanotubes partially filled with WO_{3-x} (Figure 10) and traces of Pb. The WSe₂ nanotubes had dimensions comparable to those of WS₂.

4. CONCLUSIONS

A fundamentally new method for the synthesis of MoS₂ nanotubes has been reported, based on the exposure of a

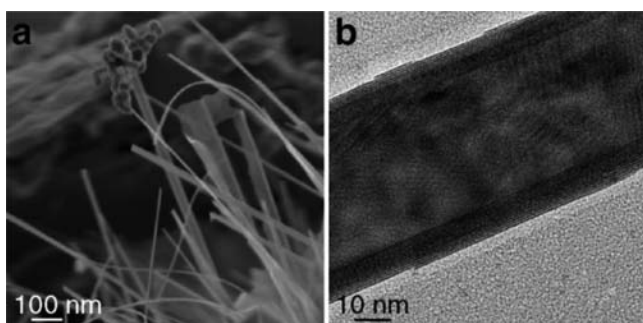


Figure 10. WSe₂ nanotubes after irradiation of the precursors for 600 s. (a) SEM image. (b) TEM image.

mixture of MoS₂ and Pb/PbO to highly concentrated sunlight. The method can be considered as a photothermally induced chemical transformation with no apparent photochemical character. The nanotubes grew from MoS₂ platelets and were partially filled with molybdenum suboxide. Nanotube length varied from 100 nm to 1 μ m, and nanotube width from 15 to 80 nm. The number of layers varied from two (encapsulating a MoO_{3-x} core) to more than 30 (for the hollow-core zones). The MoS₂ nanotubes include 1–5 at % of Pb, mostly in the MoO_{3-x} core. Atomic scale resolution TEM images indicate that some of the Pb atoms replace Mo atoms in the MoS₂ lattice.

Varying irradiation time revealed that MoO_{3-x} nanowhiskers were generated during the first 30 s, and after 60 s, one to two layers of MoS₂ covered the MoO_{3-x} nanowhisker. At longer exposure times (up to 1200 s), MoO_{3-x} nanowhiskers were continuously transformed to INT-MoS₂.

Extensive characterization methods point to a three-step growth process for the MoS₂ nanotubes: (1) intense radiative heating of the MoS₂ platelets and Pb particles leads to their rapid evaporation and to the subsequent growth of MoO_{3-x} nanowhiskers the phases of which are believed to be stabilized by the Pb atoms and which later can be successfully transformed into INT-MoS₂; (2) the MoO_{3-x} nanowhiskers are rapidly covered by a continuous shell of 2–3 MoS₂ layers; and (3) the inner MoO_{3-x} phase is continuously transformed into MoS₂ nanotubes starting at the platelets and progressing to their closed end.

Solar ablation experiments also produced similar MoSe₂, WS₂ and WSe₂ nanotubes from their respective precursors (apparently including Pb mediation via the corresponding suboxides). The MoSe₂ nanotube dimensions were comparable to those of MoS₂ nanotubes, although the WS₂ and WSe₂ nanotubes were much longer than the MoS₂ nanotubes. In all cases, the nanotubes were partially filled with corresponding suboxide and trace quantities of Pb. These findings bode well for the prospect of synthesizing INTs from other INT-metal chalcogenides that, based on their layered crystal structure, should be realizable, but have not yet been achieved experimentally. The opto-mechanical design of the solar furnace can be markedly scaled up, as evidenced by similar facilities up to 4 orders of magnitude larger in collection and target area.^{45,48} The degree to which the reactor as well as the reactions and their yields would then scale is not straightforward due to the nonlinear nature of the flux transfer and of the impact of annealing regions with strong flux and temperature gradients on the reactions, a topic to be explored in future investigations.

■ AUTHOR INFORMATION

Corresponding Author

reshef.tenne@weizmann.ac.il

Notes

The authors declare no competing financial interest.

■ ACKNOWLEDGMENTS

This research was supported by Israel Science Foundation First Program Grant No. 469/11. R.T. is also supported by the ERC INTIF grant. He holds the Drake Family Chair in Nanotechnology and is the director of the Helen and Martin Kimmel Center for Nanoscale Science. We are grateful for the support

of the Harold Perlman Foundation, and the Irving and Cherna Moskowitz Center for Nano and Bio-Nano Imaging.

■ REFERENCES

- (1) Tenne, R.; Margulis, L.; Genut, M.; Hodes, G. *Nature* **1992**, *360*, 444–446.
- (2) Margulis, L.; Salitra, G.; Tenne, R.; Talianker, M. *Nature* **1993**, *365*, 113–114.
- (3) Nath, M.; Rao, C. *J. Am. Chem. Soc.* **2001**, *123*, 4841–4842.
- (4) Schuffenhauer, C.; Popovitz-Biro, R.; Tenne, R. *J. Mater. Chem.* **2002**, *12*, 1587–1591.
- (5) Schuffenhauer, C.; Parkinson, B.; Jin Phillip, N.; Joly Pottuz, L.; Martin, J.; Popovitz Biro, R.; Tenne, R. *Small* **2005**, *1*, 1100–1109.
- (6) Popovitz-Biro, R.; Sallacan, N.; Tenne, R. *J. Mater. Chem.* **2003**, *13*, 1631–1634.
- (7) Popovitz-Biro, R.; Twersky, A.; Hacohen, Y.; Tenne, R. *AIP Conf. Proc.* **2000**, *544*, 441–447.
- (8) Levi, R.; Bar-Sadan, M.; Albu-Yaron, A.; Popovitz-Biro, R.; Houben, L.; Shahar, C.; Enyashin, A.; Seifert, G.; Prior, Y.; Tenne, R. *J. Am. Chem. Soc.* **2010**, *132*, 11214–11222.
- (9) Albu Yaron, A.; Arad, T.; Popovitz Biro, R.; Bar Sadan, M.; Prior, Y.; Jansen, M.; Tenne, R. *Angew. Chem., Int. Ed.* **2005**, *44*, 4169–4172.
- (10) Remskar, M.; Skraba, Z.; Cleton, F.; Sanjines, R.; Levy, F. *Appl. Phys. Lett.* **1996**, *69*, 351–353.
- (11) Remskar, M.; Mrzel, A.; Virsek, M.; Godec, M.; Krause, M.; Kolitsch, A.; Singh, A.; Seabaugh, A. *Nanoscale Res. Lett.* **2010**, *6*, 26.
- (12) Yella, A.; Mugnaioli, E.; Panthöfer, M.; Therese, H. A.; Kolb, U.; Tremel, W. *Angew. Chem., Int. Ed.* **2009**, *48*, 6426–6430.
- (13) Radovsky, G.; Popovitz-Biro, R.; Staiger, M.; Gartsman, K.; Thomsen, C.; Lorenz, T.; Seifert, G.; Tenne, R. *Angew. Chem., Int. Ed.* **2011**, *50*, 12316–12320.
- (14) Feldman, Y.; Frey, G.; Homyonfer, M.; Lyakhovitskaya, V.; Margulis, L.; Cohen, H.; Hodes, G.; Hutchison, J.; Tenne, R. *J. Am. Chem. Soc.* **1996**, *118*, 5362–5367.
- (15) Feldman, Y.; Zak, A.; Popovitz-Biro, R.; Tenne, R. *Solid State Sci.* **2000**, *2*, 663–672.
- (16) Zak, A.; Sallacan-Ecker, L.; Margolin, A.; Genut, M.; Tenne, R. *Nano* **2009**, *4*, 91–98.
- (17) Magneli, A. *Ark. Kemi* **1950**, *1*, 513–523.
- (18) Sahle, W. *J. Solid State Chem.* **1982**, *45*, 324–333.
- (19) Zak, A.; Feldman, Y.; Alperovich, V.; Rosentsveig, R.; Tenne, R. *J. Am. Chem. Soc.* **2000**, *122*, 11108–11116.
- (20) Feldman, Y.; Wasserman, E.; Srolovitz, D.; Tenne, R. *Science* **1995**, *267*, 222–225.
- (21) Chen, J.; Li, S.-L.; Xu, Q.; Tanaka, K. *Chem. Commun.* **2002**, 1722–1723.
- (22) Merchan-Merchan, W.; Saveliev, A. V.; Kennedy, L. A. *Chem. Phys. Lett.* **2006**, *422*, 72–77.
- (23) Handa, H.; Abe, T.; Suemitsu, M. *e-J. Surf. Sci. Nanotechnol.* **2009**, *7*, 307–310.
- (24) Cariati, F.; Bart, J. C. J.; Sgamellotti, A. *Inorg. Chim. Acta* **1981**, *48*, 97–103.
- (25) Portemer, F.; Sundberg, M.; Kihlborg, L.; Figlarz, M. *J. Solid State Chem.* **1993**, *103*, 403–414.
- (26) Frey, G. L.; Rothschild, A.; Sloan, J.; Rosentsveig, R.; Popovitz-Biro, R.; Tenne, R. *J. Solid State Chem.* **2001**, *162*, 300–314.
- (27) Kihlborg, L. *Acta Chem. Scand.* **1960**, *14*, 1612–22.
- (28) Yamazoe, N.; Ekstrom, T.; Kihlborg, L. *Acta Chem. Scand., Ser. A* **1975**, *29*, 404–8.
- (29) Kihlborg, L. *Acta Chem. Scand.* **1969**, *23*, 1834–1835.
- (30) Hu, J.; Odom, T.; Lieber, C. *Acc. Chem. Res.* **1999**, *32*, 435–445.
- (31) Lauhon, L. J.; Gudiksen, M. S.; Lieber, C. M. *Philos. Trans. R. Soc. London, Ser. A* **2004**, *362*, 1247–1260.
- (32) Bethune, D. S.; Klang, C. H.; de Vries, M. S.; Gorman, G.; Savoy, R.; Vazquez, J.; Beyers, R. *Nature* **1993**, *363*, 605–607.
- (33) Hacohen, Y. R.; Popovitz-Biro, R.; Grunbaum, E.; Prior, Y.; Tenne, R. *Adv. Mater. (Weinheim, Ger.)* **2002**, *14*, 1075–1078.
- (34) Iijima, S.; Ichihashi, T. *Nature* **1993**, *363*, 603–605.
- (35) Thess, A.; Lee, R.; Nikolaev, P.; Dai, H.; Petit, P.; Robert, J.; Xu, C.; Lee, Y. H.; Kim, S. G.; Rinzler, A. G.; Colbert, D. T.; Scuseria, G. E.; Tománek, D.; Fischer, J. E.; Smalley, R. E. *Science* **1996**, *273*, 483–487.
- (36) Wiesel, I.; Arbel, H.; Albu-Yaron, A.; Popovitz-Biro, R.; Gordon, J. M.; Feuermann, D.; Tenne, R. *Nano Res.* **2009**, *2*, 416–424.
- (37) Afanasiev, P.; Geantet, C.; Thomazeau, C.; Jouget, B. *Chem. Commun.* **2000**, 1001–1002.
- (38) Levy, M.; Albu Yaron, A.; Tenne, R.; Feuermann, D.; Katz, E. A.; Babai, D.; Gordon, J. M. *Isr. J. Chem.* **2010**, *50*, 417–425.
- (39) Chibante, L. P. F.; Thess, A.; Alford, J. M.; Diener, M. D.; Smalley, R. E. *J. Phys. Chem.* **1993**, *97*, 8696–8700.
- (40) Fields, C. L.; Pitts, J. R.; Hale, M. J.; Bingham, C.; Lewandowski, A.; King, D. E. *J. Phys. Chem.* **1993**, *97*, 8701–8702.
- (41) Flamant, G.; Luxembourg, D.; Robert, J. F.; Laplaze, D. *Sol. Energy* **2004**, *77*, 73–80.
- (42) Laplaze, D.; Bernier, P.; Flamant, G.; Lebrun, M.; Brunelle, A.; Della-Negra, S. *J. Phys. B: At., Mol. Opt. Phys.* **1996**, *29*, 4943–4954.
- (43) Alvarez, L.; Guillard, T.; Sauvajol, J. L.; Flamant, G.; Laplaze, D. *Appl. Phys. A: Mater. Sci. Process.* **2000**, *70*, 169–173.
- (44) Laplaze, D.; Bernier, P.; Maser, W. K.; Flamant, G.; Guillard, T.; Loiseau, A. *Carbon* **1998**, *36*, 685–688.
- (45) Flamant, G.; Ferriere, A.; Laplaze, D.; Monty, C. *Sol. Energy* **1999**, *66*, 117–132.
- (46) Albu Yaron, A.; Arad, T.; Levy, M.; Popovitz Biro, R.; Tenne, R.; Gordon, J. M.; Feuermann, D.; Katz, E. A.; Jansen, M.; Muehle, C. *Adv. Mater.* **2006**, *18*, 2993–2996.
- (47) Albu Yaron, A.; Levy, M.; Tenne, R.; Popovitz-Biro, R.; Weidenbach, M.; Bar-Sadan, M.; Houben, L.; Enyashin, A. N.; Seifert, G.; Feuermann, D.; Katz, E. A.; Gordon, J. M. *Angew. Chem., Int. Ed.* **2011**, *50*, 1810–1814.
- (48) Flamant, G.; Robert, J. F.; Marty, S.; Gineste, J. M.; Giral, J.; Rivoire, B.; Laplaze, D. *Energy* **2004**, *29*, 801–809.